Dynamic Three-Dimensional Lift Planning for Intelligent Boom Cranes

Zheshuo Zhang ⬤ , *Member, IEEE*, Bangji Zhang ⬤ , Wen Hu ⬤ , Rui Zhou ⬤ ,
Dongpu Cao ⬤ , *Member, IEEE*, and Hui Yin ⬤ , *Member, IEEE*

Abstract—Manually planning a crane's lifting path is complicated and laborious since it typically depends on the planner's experience. We examined dynamic three-dimensional lift planning, including problem formulation for multiobjective planning and problem-solving with an improved A* algorithm. First, we quantified various feasible movements by introducing energy and time consumption models to determine the most efficient and quickest path. Second, we examined a new method for determining the visible lifting path in Configuration space (C-space) and derived an obstacle enveloping method for collision detection in C-space. Our method is both safe and feasible. Finally, we proposed an improved A* algorithm for lift planning considering multiple objectives and featuring better computational efficiency. The experimental and simulation results demonstrate that the proposed lift planning method can comprehensively consider multiple objectives, thus providing a high-quality path for actual lifting. Furthermore, compared with the ordinary A* algorithm, the improved A* algorithm had better computational efficiency and consumed less energy and time. To our best knowledge, this is the first novel algorithm for planning crane lifts considering energy consumption and visibility in C-space.

Index Terms—Boom crane, energy conservation, graph search algorithm, lift planning.

I. INTRODUCTION

THE rapid development of mechatronics technology assists research works in meeting the global market's demand for intelligent cranes [1], [2], [3]. Crane lift planning involves complicated decisions that meet various standards and constraints [4]. These decisions can be time-consuming and largely depend on the experiences of human planners [5]. Automatic lift planning for cranes is a promising tool for improving the safety and efficiency of the crane lifting process [6].

Early studies [7], [8], [9] explored visualization-based methods to help human planners understand spatial conflicts between cranes and their surroundings. However, this method serves as an auxiliary tool, rather than a method for determining the best lifting path [10]. In contrast, *dynamic lift planning* is to automatically determine a collision-free path from the start to the goal within a limited crane operation space based on map data [11], [12], [13].

The shortest path is not always the best path, which depends on lift objectives and constraints. Prior automation planning was originated in mathematics and robotics and focused on the shortest path but without considering the crane's movements [13], [14], [15], [16]. As a result, the planned path may include many operations, some potentially unsuitable for use with cranes. Hu et al. [17] disputed that a crane's movements differ from those of robots and emphasized that *operation-friendly* also should be considered to determine the feasible path. An et al. [18] also argued that movement changes should be minimized to simplify path planning. In addition, operator-specific factors affect path quality [19]. Poor *visibility* reduces *efficiency* because additional *safety* confirmation is required during operation. To improve the quality of planned paths, the *time efficiency*, *safety*, *ease of operation*, and *visibility* should be considered. Despite mounting pressures caused by increasing energy costs, the problem of *energy efficiency* during crane lifting has not been sufficiently studied [4], [6], [9]. Future studies will inevitably combine these factors to generate a quality planning model.

Past researchers used different algorithms for lift planning [20], including nature-inspired [15], [21], [22], sampling [11], [12], [13], [17], and graph search-based algorithms [14], [16], [23], [24]. Nature-inspired algorithms, such as genetic algorithm (GA), are unsuitable for lifting tasks in various environments as they usually have difficulty justifying convergence speed and parameter sensitivity [21]. Sampling-based algorithms, such as Rapidly-exploring Random Trees (RRT), can plan robotic paths

with high degrees of freedom (DOFs) [17]. Nevertheless, determining the optimal solution is not guaranteed, and a collision detection algorithm is required for every sampling point [25]. Free from the above limitations, graph search algorithms (such as the A* algorithm) are generally simple, logical, and relatively easy to implement. Some researchers have attempted to improve the A* algorithm's computational efficiency. For example, the weighted A* multiplies the heuristic by a constant factor [29]. Another improvement is ARA*, which quickly identifies a suboptimal solution using a loose bound, then progressively tightens the bound over time [29]. This kind of efficiency improvement sacrifices optimality. The A* algorithm's computing time grows exponentially in dimensions. If the search space dimension can be reduced or the grid map search symmetry problem can be solved, then the A* algorithm's computational efficiency could be improved without sacrificing optimality.

Searching space is important when planning crane lifting paths. Generally, path search algorithms generate straight lines in space. Compared to the Configuration space (i.e., C-space), straight lines produced from Cartesian coordinates result in more complex operations [17]. A straight line formed by C-space represents the crane's actual motion, but it formed by Cartesian coordinates necessitates frequent switching during operation. Therefore, the algorithm should search the C-space for the *ease of operation*. In 2002, Soltani et al. [14] compared the results of different path search algorithms in Cartesian coordinates. Later, Reddy et al. [23] borrowed the C-space concept from the field of robot. Subsequently, many studies [12], [13], [15], [16], [23], [24] adopted planning concepts based on C-space. In 2021, Hu et al. [17] argued that both Cartesian coordinates (to determine *path visibility*) and C-space (to generate an *operation-friendly* lifting path) should be applied during planning. The application of multiple coordinates complicates and prolongs the planning process. A method of determining the *path visibility* in C-space allows for simultaneous consideration of *ease of operation* and *path visibility* in a single space.

To this end, we propose a dynamic three-dimensional (3-D) lift planning method to automatically determine the lift path after automatically considering multiple factors. We used C-Space as the search space for considering ease of operation. By deliberately introducing energy and time consumption models, the available motion in each step can be quantified and analyzed. We developed and applied a method for determining the *visibility* in C-space to the time consumption model. Using this method, attempts to improve lift path efficiency will reduce the invisible parts of the path. The lifting constraints were investigated and, once in mathematical form, we used the enveloping method to describe relevant C-Space constraints. A collision-free path in C-space assures *safety* and *ease of operation*. A cost function is formulated based on energy and time consumption models. A dimension reduction from 3-D to two dimensions (2-D) is proposed based on the projected subpath, forming the foundation of an improved A* algorithm. The proposed dynamic crane lift planning implements this improved A* to minimize the cost function and determines the optimal crane configuration sequence. This sequence can lift the payload from the start to the goal with constraints and includes path and motion information.
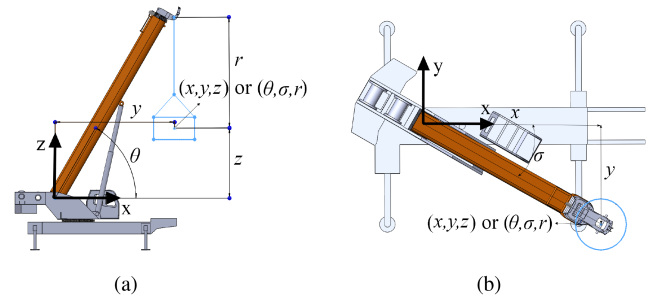

Fig. 1. Description of payload position by Cartesian coordinates and C-space. (a) Front view. (b) Top view.

The contribution of this article is to propose a dynamic lift planning method that considers the *energy- and time efficiency* while satisfying the requirements of *safety*, *ease of operation,* and *visibility*. This work fills the following three research gaps.
1) Our method accounts for the energy and time consumption when lift planning.
2) Our method considers visibility and ease of operation in a single coordinate.
3) Our method improves the computational efficiency of the A* algorithm by dimension reduction for crane lift planning.

Experimental verification was performed with a real crane.

II. PROBLEM FORMULATION

This article deals with automatic 3-D lift planning and considers multiple objectives, rather than a simple "shortest path" to determine the optimal collision-free path for crane operation. Based on assumptions and coordinates, the crane lift planning problem is described mathematically with cost function and constraints. The following common assumptions are considered [17], [18], [21].
1) Cranes are not allowed to drive while lifting payload.
2) Booms may not extend or retract while lifting payload.
3) The payload's rotation is uncontrolled; consequently, the payload's shape is ignored (the payload is conservatively simplified by a cylinder along the z-axis).
4) The payload's sway can be represented by a payload cylinder with a larger radius, and thus ignored.
5) Steady velocity of the same action is constant.
6) The crane boom should not be located under noticeable obstacles (the crane may work under a roof only if a roof is beyond the scope of the crane's boom).
7) Obstacles in the lifting area are stationary.
8) Compound operations are not permitted.

A. Cartesian Coordinates and C-Space

Based on assumption 1), we can describe the payload's center position using the absolute position in Cartesian coordinates by $(x, y, z) \in \mathbb{R}^3$, as shown in Fig. 1. The C-space refers to the collection of all possible configurations of boom crane in various postures [24], including three elements: 1) the luffing angle $\theta \in [0°, 90°]$, 2) the slewing angle $\sigma \in [0°, 360°)$, and 3)

the hoisting length of the sling $r \in \mathrm{R}^+$. Therefore, the C-space for a boom crane with three DOFs is a 3-D space with (θ, δ, r) for crane posture configuration, as shown in Fig. 1. Boom length L_b is constant according to assumption 2). The two descriptions of the payload position can be converted into one another as follows:

$$\begin{cases} \theta = \arccos\left(\sqrt{x^2 + y^2}/L_b\right) \\ \sigma = \arctan\left(y/x\right) \\ r = L_b \sin\theta - z \end{cases} \quad (1)$$

$$\begin{cases} x = L_b \cos\theta \cos\sigma \\ y = L_b \cos\theta \sin\sigma \\ z = L_b \sin\theta - r \end{cases} \quad (2)$$

B. Crane Lift Planning Problem

The crane lift planning problem can be written as

$$\min\left(J = \alpha_t \tilde{F}_t + \alpha_e \tilde{F}_e\right)$$

$$\text{Constraints} \begin{cases} \text{path} \in \Pi \\ \text{collision-free in C-Space} \end{cases} \quad (3)$$

where J is the cost function of the lifting path, $\tilde{F}_t$ and $\tilde{F}_e$ represent normalized time and energy consumption, α_t and α_e correspond to weights for energy and time consumption, respectively, and Π indicates the crane working area.

Remark 1: Equation (3) considers *energy and time efficiency* while satisfying *safety*, *ease of operation*, and *visibility*. Improvements in *energy and time efficiency* that result from the shorter path length may be offset by extra energy costs and reduced operating speeds. It is worth exploring how to choose a path that minimizes energy and time consumption.

Remark 2: *Safety*, *ease of operation*, and *visibility* can be implied by solving for the minimum energy and time consumption within the constraints. The first constraint means that there is a working area Π for any selected crane and working outside Π will affect *safety*; thus, it is forbidden. The second constraint requires that there is no collision in C-space, which indicates both *safety* and *ease of operation*. Poor *visibility* will cause operators to slow down the crane's movements to maximize operational safety; thus, *visibility* can be included in the time consumption calculation F_t.

III. ENERGY AND TIME CONSUMPTION MODELS

This section proposes energy and time consumption models for boom cranes. These models provide a solid foundation for selecting a lift path, from all feasible lift paths, that requires the least energy and time.

A. Energy Consumption Model

The energy F_e consumed by the crane while lifting is three-fold: energy converted into kinetic energy E_k and potential energy E_p, and energy needed to overcome traction resistance E_f. Other sources of energy consumption, such as the crane's

electrical circuits, were relatively small and, therefore, ignored

$$F_e = E_k + E_p + E_f. \quad (4)$$

Cranes lose kinetic energy while deceleration. Based on assumption 5), the steady velocity for luffing $\dot{\theta}_{\mathrm{st}}$, slewing $\dot{\sigma}_{\mathrm{st}}$, and hoisting $\dot{r}_{\mathrm{st}}$ are constants. The crane's kinetic energy E_k can be expressed as

$$E_k = n_\theta \left(\frac{1}{2} I_y \dot{\theta}_{\mathrm{st}}^2 + \frac{1}{2} m \left(L_b \dot{\theta}_{\mathrm{st}}\right)^2\right)$$

$$+ n_\sigma \left(\frac{1}{2} I_z \dot{\sigma}_{\mathrm{st}}^2 + \frac{1}{2} m (L_b \dot{\sigma}_{\mathrm{st}})^2\right) + n_r \left(\frac{1}{2} m \dot{r}_{\mathrm{st}}^2\right)$$

$$= n_\theta E_\theta + n_\sigma E_\sigma + n_r E_r \quad (5)$$

where I_y and I_z denote the moments of boom inertia when luffing and slewing, respectively. The kinetic energy costs of each luffing E_θ, slewing E_σ, and hoisting E_r are constant. Consequently, the total kinetic energy cost depends on the switching times of luffing n_θ, slewing n_σ, and hoisting n_r. Both luffing and hoisting change potential energy while slewing will not. The energy consumption attributed to potential energy can be written as

$$E_p = \int D(d\sin\theta)(MgL_C + mgL_b)d\sin\theta$$

$$+ \int D(-dr)mgdr \quad (6)$$

where $D(\cdot) = (\mathrm{sign}(\cdot) + 1)/2$, and $\mathrm{sign}(\cdot)$ is the signum. M is the boom's mass. Its center of gravity is located at L_C. The potential energies of sling and hook were relatively small and, therefore, ignored. The potential energies at the start and goal are constant and independent of the path. Nevertheless, the potential energy cost of various paths could differ for a job. The crane consumes energy when raising payloads or booms but it cannot recover energy when lowering them.

The boom crane usually consists of two parts: 1) the undercarriage (or the lower) and 2) the superstructure (or upper which includes the boom). The lower and the upper are coupled via a turntable, allowing the upper to slew from side to side. The energy consumed during slewing accounts for the main energy lost due to friction resistance, which can be expressed as

$$E_f = \int \left(u L_b \left(\frac{M}{2} + m\right) g \cos\theta\right) d\sigma \quad (7)$$

where u is a constant related to the friction coefficient. The friction resistance during luffing originates from the boom's joints and luffing cylinder while the friction resistance during hoisting originates from the hoist pulley. Compared with the potential energy cost, friction resistance energy cost during luffing and hoisting is relatively small, and was, therefore, ignored when selecting the path that consumes the least energy.

B. Path Selection Based on the Energy Consumption Model

By eliminating compound operations, we can identify six basic motions for a configuration $(\theta_c, \sigma_c, r_c)$ in C-space, as
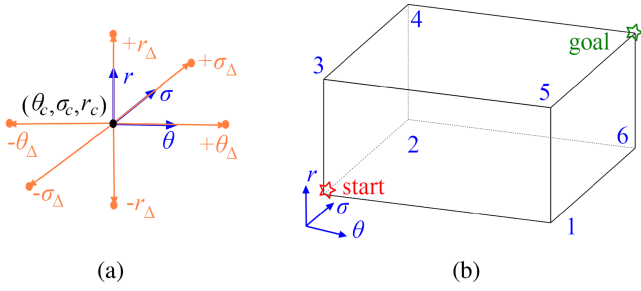
Fig. 2.　Basic motions and paths in C-space.

Fig. 3.　Paths for an operation in (a) C-space and (b) Cartesian coordinates.

shown in Fig. 2(a). Energy consumed for these basic motions can be expressed as

$$E_{+\theta\Delta} = s_\theta E_\theta + k_1 \left(\sin(\theta_c + \theta_\Delta) - \sin\theta_c \right) \tag{8}$$

$$E_{-\theta\Delta} = 0 \tag{9}$$

$$E_{+\sigma\Delta} = s_\sigma E_\sigma + k_2 \sigma_\Delta \cos\theta_c \tag{10}$$

$$E_{-\sigma\Delta} = s_\sigma E_\sigma + k_2 \sigma_\Delta \cos\theta_c \tag{11}$$

$$E_{+r\Delta} = 0 \tag{12}$$

$$E_{-r\Delta} = s_r E_r + k_3 r_\Delta \tag{13}$$

where $k_1 = (M/2 + m)gL_b$, $k_2 = \mu(M/2 + m)gL_b$, and $k_3 = mg$. The values of s_θ, s_σ, and s_r are 1 or 0, standing for the motion switches into luffing, slewing, and hoisting or not, respectively. For $+\theta_\Delta$ and $-r_\Delta$, kinetic energy or friction resistance can be converted from potential energy, rather than a power system, thus $E_{+r\Delta} = E_{-\theta\Delta} = 0$.

In Fig. 2(b), without the influence of obstacles, there are six basic paths from the start to the goal, as follows.

1) Path 1: start → Node 1→Node 6→goal.
2) Path 2: start → Node 2→Node 6→goal.
3) Path 3: start → Node 1→Node 5→goal.
4) Path 4: start → Node 2→Node 4→goal.
5) Path 5: start → Node 3→Node 4→goal.
6) Path 6: start → Node 3→Node 5→goal.

If the path length is considered the only objective, all six paths have the same cost. However, when energy consumption is considered, Paths 1, 3, and 6 are better than Paths 2, 4, and 5. Moreover, from (10) and (11), it can be found that the consumed energy is positively correlated with $\cos\theta_c$. Energy can be saved by slewing at a large luffing angle; "Node 1→Node 6" and "Node 5→goal" cost less energy than "start → Node 2" and "Node 3→Node 4." This indicates that the energy consumption model determines the most energy-efficient path among available options, thus breaking the symmetry problem during the grid map search.

C. Time Consumption Model

The crane time cost F_t during the lifting process is threefold: 1) time spent in steady motion T_1, 2) extra time spent in switch motion due to acceleration and deceleration T_2, and 3) extra time spent moving slowly in an invisible area T_3
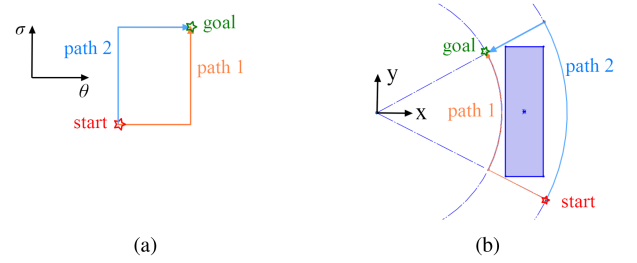
$$F_t = T_1 + T_2 + T_3. \tag{14}$$

Time spent during steady motion T_1 on a given path can be determined by each motion's steady velocity as

$$T_1 = \frac{\theta}{\dot\theta_{\mathrm{st}}} + \frac{\sigma}{\dot\sigma_{\mathrm{st}}} + \frac{r}{\dot r_{\mathrm{st}}}. \tag{15}$$

We assume that extra time needed for acceleration and deceleration for luffing T_θ, slewing T_σ, and hoisting T_r are constant. Accordingly, T_2 is determined by switch times as

$$T_2 = n_\theta T_\theta + n_\sigma T_\sigma + n_r T_r. \tag{16}$$

It is assumed that the extra time spent per unit length due to the invisibility for luffing Υ_θ, slewing Υ_σ, and hoisting Υ_r is constant. After determining the invisible portions for luffing θ_{iv}, slewing σ_{iv}, and hoisting r_{iv}, the extra time spent moving slowly in the invisible area T_3 can be calculated by

$$T_3 = \Upsilon_\theta \theta_{\mathrm{iv}} + \Upsilon_\sigma \sigma_{\mathrm{iv}} + \Upsilon_r r_{\mathrm{iv}}. \tag{17}$$

D. Path Selection Based on the Time Consumption Model

Herein, we propose a method for determining the *visibility* in C-space. The operation is illustrated in Fig. 3. The operator is located at the original coordinates. There are two possible paths from the start to the goal, as shown in Fig. 3(a). Path *visibility* can be inferred from Fig. 3(b), which indicates that the slewing process of Path 2 is blocked.

Theorem 1: If (θ_o, σ_o) belongs to obstacle, $(\theta_o - \theta_\lambda, \sigma_o)$ is invisible for any $\theta_\lambda > 0$.

Proof: In Cartesian coordinates, (x_o, y_o) corresponds to (θ_o, σ_o), and $(x,' y')$ corresponds to $(\theta_o - \theta_\lambda, \sigma_o)$. The point-slope form of a straight line passing through the origin and (x_o, y_o) can be described by

$$(y_o - 0)/(x_o - 0) = \tan\sigma_o. \tag{18}$$

According to (1), there are $x' = L_b \cos(\theta_o - \theta_\lambda)\sin\sigma_o$ and $y' = L_b \cos(\theta_o - \theta_\lambda)\cos\sigma_o$. The point-slope form of a straight line passing the origin and (x_o, y_o) can be derived as

$$(y' - 0)/(x' - 0) = \tan\sigma_o. \tag{19}$$

Equations (18) and (19) indicate that (x_o, y_o) and $(x,' y')$ form a straight line passing the origin. In addition

$$|x'| = |L_b \cos(\theta_o - \theta_\lambda)\sin\sigma_o| > |L_b \cos\theta_o \sin\sigma_o| = |x_o| \tag{20}$$
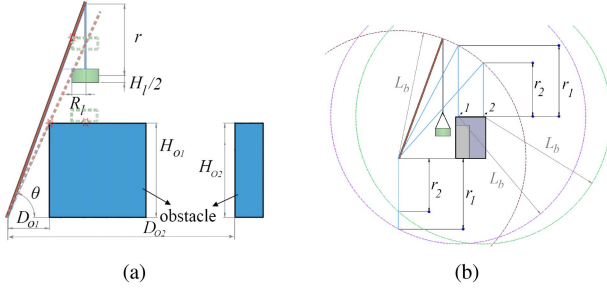
Fig. 4. Possible collision among boom, obstacle and payload.

meaning that the line of sight from the origin to $(x,' y')$ will be blocked by (x_o, y_o). ∎

Based on Theorem 1, slewing at a smaller luffing angle is more likely to be invisible. Consequently, in Fig. 3, Path 1 is better than Path 2. The time consumption model can determine the most time-efficient path among all the available options.

Remark 3: The actual energy and time costs may differ from the energy and time consumption models established here. Nevertheless, these differences in costs depend on factors like operating skill, which would not affect a general selection of the quickest or most efficient path. In other words, the proposed models are sufficient for guiding path selection by ranking each movement's available choices.

IV. LIFT PLANNING

In this section, we construct constrained C-space and propose a method for lift planning that considers multiple objectives and features better computational efficiency.

A. Constraints

Lifting constraints in C-space are proposed considering the crane's working area, collisions, and obstacles. A table of crane working areas Π_θ is an essential document for crane operators. These tables display the maximum bearable payload mass m and boom length L_b applicable to the relevant work. The first constraint in (3) limits the luffing angle θ and is expressed as

$$\theta \in \Pi_\theta (m, L_b). \tag{21}$$

The second constraint in (3) relates to all possible collisions among the boom, obstacle, and payload, as shown in Fig. 4.

1) Collision Between the Payload and Boom: In Fig. 4(a), if the payload has a large radius R_l, the payload may collide with the boom when it is hoisted up high (small r) or when the boom is luffed upright (large θ). Considering possible collisions between the payload and boom, there is a limit value for the minimum sling length r

$$r > R_l \tan\theta + \frac{H_l}{2}. \tag{22}$$

2) Collision Between the Boom and Obstacles: In Fig. 4(a), some obstacles may be high and close to the luffing center. The boom could collide with the obstacle when the luffing angle was small. The slewing angle σ determines the luffing plane of the boom. As it should be, obstacles are located by both θ
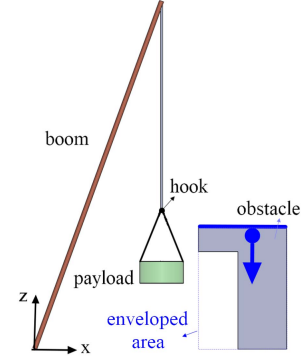

Fig. 5. Enveloping obstacle from the top in a vertical direction.

and σ. The height for the ith obstacle is $H_{oi}(\sigma)$ and its distance to the luffing center is $D_{oi}(\sigma)$. Considering possible collisions between the boom and obstacles, there is a limit value for the minimum luffing angle θ (related to slewing angle σ) as

$$\theta(\sigma) > \max\left(\arctan\frac{H_{oi}(\sigma)}{D_{oi}(\sigma)}\right). \tag{23}$$

3) Collision Between Payload and Obstacles: Fig. 4(b) illustrates the method to determine the vertical distance between the boom tip and the top of the obstacle. The top of the obstacle could have various heights $H_o(\theta, \sigma)$, determined by both θ and σ. The payload would touch the obstacle surface when the sling was too long. Considering possible collisions between the payload and obstacles, there is a maximum limit of sling length related to both the luffing angle θ and the slewing angle σ as

$$r(\theta, \sigma) < L_b \sin\theta - H_o(\theta, \sigma) - \frac{H_l}{2}. \tag{24}$$

C-space constraints can be expressed by (21)–(24). These constraints manifest as impassable areas; the lifting path is searchable outside these areas.

B. Enveloped Obstacles

An enveloping method is proposed for two purposes: 1) to simplify lift planning by examining lifting characteristics and 2) to account for the payload's size and sway by a larger obstacle area considering the boom crane's movements.

Lifting characteristics: The boom tip cannot be lower than any obstacles considered as shown in assumption 6). Consequently, there will be no obstacles beyond the boom tip on the map. As shown in Fig. 5, The sling connecting the payload and the boom tip limits the payload's path below any obstacle, causing the obstacles to be enveloped vertically from the top. Consequently, Lemma 1 is proposed.

Lemma 1: In C-space, if $r_i(\theta, \sigma)$ is impassable, then for any $r_j > r_i$, $r_j(\theta, \sigma)$ is impassable.

Based on Lemma 1, a higher space will distribute fewer obstacles on the map. Consequently, the path in Fig. 2(b) including "Node 1→Node 6" (rather than "Node 5→goal") is more likely to be clear, because its luffing and slewing occur on a higher horizontal plane (smaller r). Consequently, Path 1 is the best among the six basic paths. This conclusion provides a
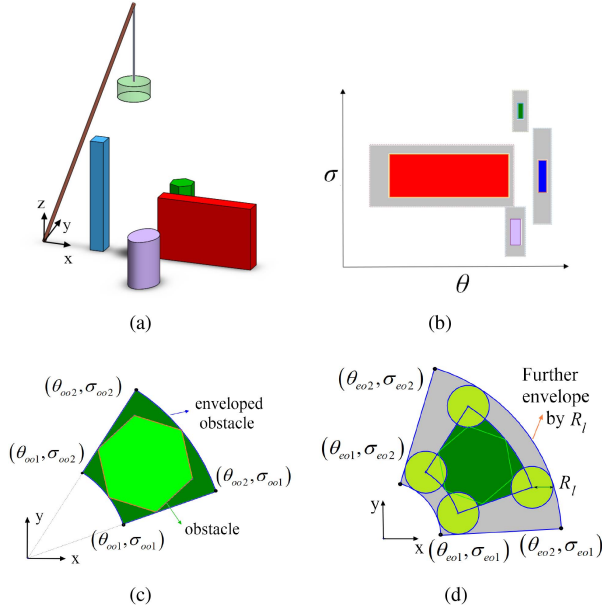
Fig. 6. Enveloped obstacle and payload radius in two different coordinates.

potential solution for the path symmetry problem posed by the A* algorithm.

Motion Characteristics: Luffing or slewing draws an arc in Cartesian coordinates with the boom origin as the center. Inspired by the work in [18], the obstacle is tightly enveloped by a section of a hollow cylinder with vertices $(\theta_{oo1}, \sigma_{oo1})$, $(\theta_{oo1}, \sigma_{oo2})$, $(\theta_{oo2}, \sigma_{oo2})$, and $(\theta_{oo2}, \sigma_{oo1})$, as shown in Fig. 6(c). These vertices' coordinates can be determined by the minimum or maximum values of the original obstacle's coordinates.

Most path search algorithms generate only a thin line. It is easier to handle a point's movement and explain the size and sway of the payload through the extended obstacle area, rather than to find a wide path outside the original obstacles [24]. In assumptions 3) and 4), the payload's size and sway can be represented by the payload radius R_l. Consequently, further envelope extends the enveloped obstacle by R_l, forming a larger hollow cylinder with vertices, $(\theta_{eo1}, \sigma_{eo2})$, and $(\theta_{eo2}, \sigma_{eo1})$, as shown in Fig. 6(d). The vertices' coordinates of the further envelope can be calculated by

$$\begin{cases} \theta_{e01} = \arccos\left(\cos\theta_{oo1} - R_l/L_b\right) \\ \sigma_{eo1} = \sigma_{oo1} - \arctan\left(R_l/(L_b\cos\theta_{oo1})\right) \\ \theta_{eo2} = \arccos\left(\cos\theta_{oo2} + R_l/L_b\right) \\ \sigma_{eo2} = \sigma_{oo2} + \arctan\left(R_l/(L_b\cos\theta_{oo1})\right) \end{cases}. \quad (25)$$

Based on the enveloping method proposed above, the obstacles shown in Fig. 6(a) can be converted to quadrilaterals in the θ–σ plane, as shown in Fig. 6(b).

C. Improved A* Algorithm

Herein, an improved A* is enhanced in two aspects: 1) the cost function related to *energy and time efficiency*, and 2) dimension reduction for faster calculation.

1) Costs Related to Energy and Time Efficiency: When A* searches a grid map cluttered with obstacles, each grid is considered a node free or occupied by obstacles. The cost function for the kth node $f(k)$ includes the actual cost $g(k)$ from the start to the kth node and a heuristic estimate $h(k)$ of the cost to the goal, expressed as

$$f(k) = g(k) + h(k). \quad (26)$$

For the ordinary A* algorithm [16], $g(k)$ and $h(k)$ are determined by the Manhattan or Euclidean distance to obtain the shortest path. The shortest path may not necessarily preserve energy and time. We propose a new cost function related to energy and time consumption. The actual cost from the kth node to the $(k-1)$th node is expressed as

$$\begin{aligned} c_{k,k-1} &= \alpha_e \tilde{F}_{e|k,k-1} + \alpha_t \tilde{F}_{t|k,k-1} \\ &= \alpha_e \frac{F_{e|k,k-1}}{F_{eh|g,s}} + \alpha_t \frac{F_{t|k,k-1}}{F_{th|g,s}} \end{aligned} \quad (27)$$

where

$$\begin{aligned} F_{e|k,k-1} &= D\left(\theta_k - \theta_{k-1}\right) k_1 \left(\sin\theta_k - \sin\theta_{k-1}\right) \\ &\quad + k_2 \left|\sigma_{k-1} - \sigma_k\right| \cos\left(\max\left(\theta_{k-1}, \theta_k\right)\right) \\ &\quad + D\left(r_{k-1} - r_k\right) k_3 \left(r_{k-1} - r_k\right) \\ &\quad + E_\theta s_\theta + E_\sigma s_\sigma + E_r s_r \\ F_{eh|g,s} &= D\left(\theta_g - \theta_s\right) k_1 \left(\sin\theta_g - \sin\theta_s\right) \\ &\quad + k_2 \left|\sigma_s - \sigma_g\right| \cos\left(\max\left(\theta_s, \theta_g\right)\right) \\ &\quad + D\left(r_s - r_g\right) k_3 \left(r_s - r_g\right) \\ F_{t|k,k-1} &= T_\theta s_\theta + T_\sigma s_\sigma + T_r s_r + \frac{\left|\theta_k - \theta_{k-1}\right|}{\dot{\theta}_{st}} \\ &\quad + \frac{\left|\sigma_{k-1} - \sigma_k\right|}{\dot{\sigma}_{st}} + \frac{\left|r_{k-1} - r_k\right|}{\dot{r}_{st}} \\ &\quad + \Upsilon_\theta \theta_{iv|k,k-1} + \Upsilon_\sigma \sigma_{iv|k,k-1} + \Upsilon_r r_{iv|k,k-1} \\ F_{th|g,s} &= \frac{\left|\theta_k - \theta_g\right|}{\dot{\theta}_{st}} + \frac{\left|\sigma_g - \sigma_k\right|}{\dot{\sigma}_{st}} + \frac{\left|r_g - r_k\right|}{\dot{r}_{st}}. \end{aligned}$$

In them, $(\theta_k - 1, \sigma_k - 1, r_k - 1)$, $(\theta_k, \sigma_k, r_k)$, $(\theta_s, \sigma_s, r_s)$, and $(\theta_g, \sigma_g, r_g)$ are configurations for the $(k-1)$th, kth nodes, the start, and the goal, respectively. $g(k) = g(k-1) + c_{k,k-1}$, and $g(k-1)$ stands for the actual cost of the $(k-1)$th node. $g(s) = 0$. Consequently, the actual cost from the kth node $g(k)$ can be iteratively calculated as

$$g(k) = c_{k,k-1} + c_{k-1,k-2} + c_{k-2,k-3} + \cdots + c_{1,s}. \quad (28)$$

An admissible heuristic is necessary to determine the optimal path using the A* algorithm, previously verified theoretically and numerically [28]. The heuristic function considering energy and time consumption is defined as

$$\begin{aligned} h(k) &= D\left(\theta_g - \theta_k\right) k_1 \left(\sin\theta_g - \sin\theta_k\right) \\ &\quad + k_2 \left|\sigma_k - \sigma_g\right| \cos\left(\max\left(\theta_k, \theta_g\right)\right) \\ &\quad + D\left(r_k - r_g\right) k_3 \left(r_k - r_g\right) \end{aligned}$$

$$+ \frac{| \theta_k - \theta_g |}{\dot{\theta}_{\text{st}}} + \frac{| \sigma_g - \sigma_k |}{\dot{\sigma}_{\text{st}}} + \frac{| r_g - r_k |}{\dot{r}_{\text{st}}}. \quad (29)$$

If there is no obstacle blocking the path to the goal, this heuristic function equals the actual cost from the kth node to the goal.

2) Dimension Reduction: To improve the computational efficiency of the improved A* algorithm, we propose a dimension reduction method based on the projected subpath for changing the search map from 3-D (θ–σ–r) to 2-D (θ–σ). Two theorems are proposed to prove that the optimal path contains a projected 2-D subpath.

Theorem 2: Let r_m be the minimum sling length of the admissible lifting path

$$P = [N_s (\theta_s, \sigma_s, r_s), N_1 (\theta_1, \sigma_1, r_1)$$
$$N_2 (\theta_2, \sigma_2, r_2), \dots, N_g (\theta_g, \sigma_g, r_g)]. \quad (30)$$

There is always an admissible path as

$$P' = [N_s (\theta_s, \sigma_s, r_s), P'_{\text{sub}}, N_g (\theta_g, \sigma_g, r_g)] \quad (31)$$

where the subpath

$$P'_{\text{sub}} = [N'_s (\theta_s, \sigma_s, r_m), N'_1 (\theta_1, \sigma_1, r_m),$$
$$N'_2 (\theta_2, \sigma_2, r_m), \dots, N'_g (\theta_g, \sigma_g, r_m)] \quad (32)$$

is the 2-D projection of P on the plane (θ–σ) determined by r_m.

Proof: We prove Theorem 2 by assuming the contrary: P is passable, but the projection node $N'_i(\theta_i, \sigma_i, r_m) \in P'_{\text{sub}}$ is impassable. Since r_m is the minimum sling length of P, there is $r_m \leq r_i$. The original node of the projection node N'_i is $N_i(\theta_i, \sigma_i, r_i) \in P_{\text{sub}}$. According to Lemma 1, if $N'_i(\theta_i, \sigma_i, r_m)$ is impassable and $r_m \leq r_i$, then $N_i(\theta_i, \sigma_i, r_i)$ is impassable, contradicting the assumption. ∎

Theorem 3: The actual cost for P is always no less than the actual cost for P'.

Proof: From (27), the actual cost for movement in r is independent of the values of θ and σ. For P', the only movement in r happens at the beginning and end. For P, the movement in r may happen in the midpoint, and $\sum_{k=s}^{g} |r_{k-1} - r_k| \geq r_m$. Therefore, for movement in r, the actual cost for P is always no less than the actual cost for P'. In addition, the actual cost for movement in the DOF or σ is independent of the value of r. The values of θ and σ for every node in P and its projection node in P' equal, meaning that for movement in θ and σ, the actual cost for P is the same as the actual cost for P'. In summary, the actual cost for P is always no less than the actual cost for P'. ∎

Based on Theorems 2 and 3, we can conclude that the optimal path contains a 2-D subpath. For any 3-D lift planning in C-space, r decreases first, reaching the $\theta - \sigma$ plane, where fewer obstacles exist. During the 2-D planning stage, an optimized path P'_{sub} must be determined from the 2-D start (θ_s, σ_s) to the 2-D goal (θ_g, σ_g). Actually, P'_{sub} is 2-D as all nodes of P'_{sub} are all on plane r_m. $g_{g,s}^{2\text{D}}$ stand for the actual cost of P'_{sub}, which can be determined by (27). After reaching 2-D goal (θ_g, σ_g), the sling's length increases to lay the payload on the 3-D goal $(\theta_g, \sigma_g, r_g)$, finishing the plan. Consequently, 3-D planning can be simplified as 2-D planning on only a few necessary planes

---

Algorithm 1: Pseudocode for the Improved A* Algorithm.

1. Splitting grid resolution for each dimension in C-space;
2. Initializing the 3-D grid map of θ–σ–r by setting the 3-D start $(\theta_s, \sigma_s, r_s)$ and 3-D goal $(\theta_g, \sigma_g, r_g)$;
3. Initializing the Closed List by the nodes in enveloped obstacles' areas;
4. For every available r_i:
   a. Initializing the 2-D grid map by setting the 2-D start (θ_s, σ_s) and 2-D goal (θ_g, σ_g) in the θ–σ plane with r_i;
   b. Setting start as the first node of Open List;
   c. While loop
      • If Open List is empty, return False; break; remove the node "k" with the lowest $f(k)$ from the Open List;
      • Mark node "k" as parent node;
      • If node "k" is the goal, return TRUE; break;
      • For expanded neighbors "m" of node "k" on θ–σ map: if node "m" is not in Open List, push node "m" into Open List; if Node "m" is in Open List and $g(m) > g(k) + C_{m,k}$, which means a better path to node "m" is found, then update corresponding parent node of Node "m," $g(m)$ and $f(m)$ value;
5. Finding the parent node of the 2-D goal; finding the parent node of another parent node until reaching the 2-D start and forming a 2-D path;
6. Finding the r_i^* with the lowest cost J in r_i;
7. Connecting $(\theta_s, \sigma_s, r_s)$ to $(\theta_s, \sigma_s, r_i^*)$, and $(\theta_g, \sigma_g, r_i^*)$ to $(\theta_g, \sigma_g, r_g)$, respectively, resulting in an optimized 3-D path in C-space.

---

in C-space. These $\theta - \sigma$ planes can be identified by r_m, whose potential range is limited by the obstacles' heights and positions as

$$\min (r_s, r_g) \leq r_m \leq \max_{(\theta, \sigma)} \left(L_b \sin \theta - H_o (\theta, \sigma) - \frac{H_l}{2} \right). \quad (33)$$

The pseudocode for the improved A* algorithm is in Algorithm 1. In total, the cost J can be determined by

$$J = g_{g,s}^{2\text{D}} + \alpha_e \frac{k_3 (r_s - r_m) + E_r}{F_{eh|g,s}}$$
$$+ \alpha_t \frac{(| r_s - r_m | + | r_g - r_m |)/\dot{r}_{\text{st}} + 2T_r}{F_{th|g,s}}. \quad (34)$$

Remark 4: The improved A* algorithm is superior to the ordinary A* algorithm. First, the improved A* ensures the *energy and time efficiency* by a new cost function, based on the energy and time consumption models. In contrast, the ordinary A* for the shortest path may not necessarily result in the path requiring the least energy and time. Second, reducing dimensions from 3-D to 2-D was applied to the improved A*; consequently, only a few 2-D planes were searched (instead of 3-D). This improves the computational efficiency of the ordinary A* algorithm for searching in a 3-D space. These benefits will be further demonstrated through experiments and simulations.
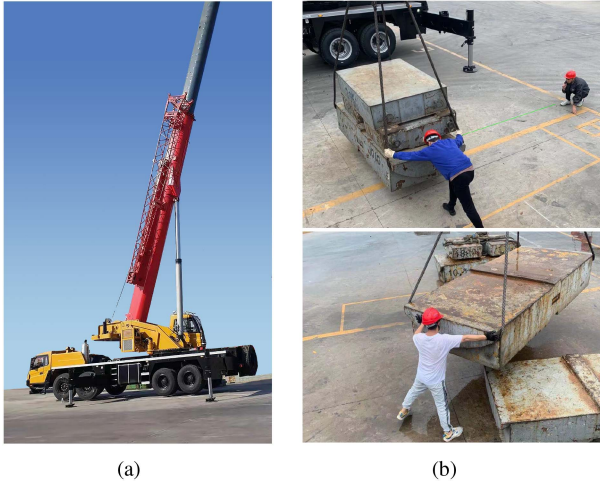
Fig. 7. Test by (a) boom crane with (b) standard weights and laser rangefinder.

TABLE I
CORRESPONDING LOADING CAPACITY OF THE BOOM CRANE USED

Work radius (m)	Maximum payload mass (t)	Minimum luffing angle (degree)
16	12	57
18	9.65	52
20	7.8	46
22	6.3	41

V. RESULTS AND DISCUSSION

A. Experimental Verification

Crane lift experiments were completed to evaluate the algorithm's energy and time consumption performance. These case studies are executed by a boom crane, as shown in Fig. 7(a). The boom mass $M = 9.87$ t. The steady velocity for luffing $\dot{\theta}_{st} = 0.5°/s$, for slewing $\dot{\sigma}_{st} = 0.5°/s$ and for hoisting $\dot{r}_{st} = 1$ m/s. $T_\theta = 10$ s, $T_\sigma = 10$ s, and $T_r = 1$ s represent the extra time spent due to acceleration and deceleration. The boom length used in the experiment is 29 m, and the corresponding loading capacity is listed in Table I. The boom's center of mass and moment of inertia vary with the boom length. Preliminary tests with standard weights and a laser rangefinder [shown in Fig. 7(b)] are conducted to determine the mass center of boom $L_C = 20.86$ m, the moment of inertia $I_y = I_z = 1.43 \times 10^6$ kg·m² based on force balance.

The 3-D environment map is digitalized using inclined aerial photography technology, as illustrated in Fig. 8(a) and (b). This job requires lifting two devices with different weights from the start to the goal. One weighs 1 t, and the other weighs 10 t. The payloads are similar in size, represented by a cylinder with a radius of $R_l = 1$ m and a height of $H_l = 1$ m. The environment map is established in C-space with the constraints, the start, and the goal. The crane lift paths for the actual job are shown in Fig. 8(c)–(f), provided by a lift planner with more than 10 years of experience. In addition, the paths searched by the improved A* algorithm with ($\alpha_e = 0.5, \alpha_t = 0.5$) are also illustrated in Fig. 8(c)–(f). The proposed method's paths were very similar to
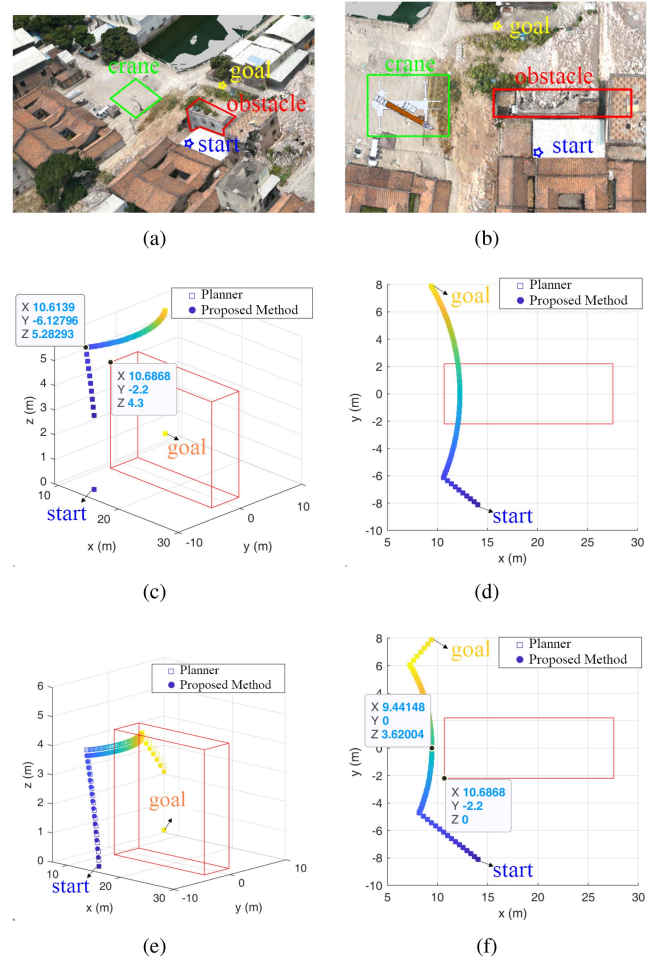

Fig. 8. Paths for different payload mass in a 3-D environment map. (a) Side view and (b) Top view for an environment map. (c) Side view and (d) Top view for a payload of 1 t. (e) Side view and (f) Top view for a payload of 10 t.

those suggested by an experienced planner. The slight difference in Fig. 8(e)–(f) is that the planner required the payload to leave the ground before luffing to avoid friction between the payload and the ground. Planners mainly considered energy and time efficiency, safety, visibility, and ease of operation. The paths' similarities demonstrate that the proposed method can comprehensively consider multiple objectives.

The paths of the 1 t payload are shown in Fig. 8(c) and (d). Luffing or slewing motion draws an arc rather than a straight line in Cartesian coordinates. It can be found that the 1-t payload is hoisted high enough to slew over the obstacle. In contrast, the path of the 10-t payload in Fig. 8(e)–(f) avoids unnecessary hoisting and bypasses the obstacle with more luffing. This signifies that the improved A* algorithm considers energy consumption. Lifting a heavy payload into a higher space consumes additional energy. This energy can be calculated by (34) and (35). In detail, the payload mass m affects the coefficients k_1, k_2, k_3, E_θ, E_σ, and E_r. For instance, when $m = 1$ t, $k_1 = 2.3 \times 10^6$; when $m = 10$ t, $k_1 = 4.86 \times 10^6$. Furthermore, the gap between the obstacle and the path in Fig. 8(c)–(f) implies the payload's radius and height envelope. Specifically, considering the 1-m vertical
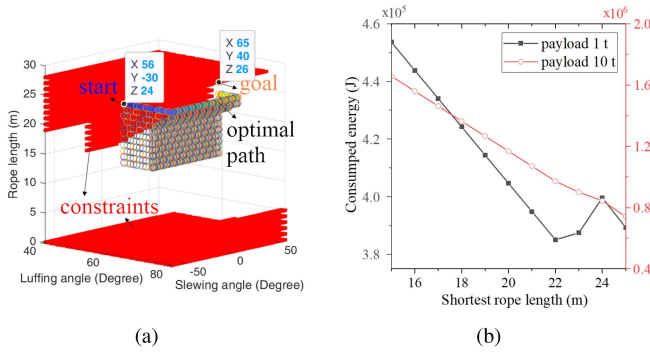
Fig. 9. (a) Paths in C-space and (b) consumed energy for different r_m by the proposed planning method.

Fig. 10. Paths of different methods in a complex environment. (a) Side view. (b) Top view.

payload envelope depicted in Fig. 8(c), slewing would occur around 5.3 m.

From Fig. 8(c) and (e), it can be noted that the payload hoisting only occurs at the path's beginning and end. The shorter the rope, the higher the payload. Based on Lemma 1, it is better to luff and slew in the plane with the minimum sling length r_m in the path. Therefore, the first step is to hoist the payload to r_m. The paths of various r_m are plotted in Fig. 9(a). The consumed energy of the 1- and 10-t payloads is illustrated in Fig. 9(b). According to (33), the minimum of r_m considered is determined by the path's start and the goal while the maximum of r_m considered is determined by the obstacle's location and height. In Fig. 9(b), the crane's minimum energy consumption is $r_m = 22$ m for a 1-t payload and $r_m = 25$ m for a 10-t payload. In detail, when r_m increases from 22 m to 24 m, the energy consumed by 1-t payload increases because each path's maximum luffing angle increases with increases of r_m to bypass the obstacle area, as shown in Fig. 9(a). In contrast, when r_m increases, the energy consumed by the 10-t payload continues to decrease since the payload is heavy. The energy consumed by hoisting the payload is greater than the energy consumed by luffing the boom.

B. Performance Analysis

Compared with the ordinary A* algorithm, RRT, and GA, the performance of the improved A* algorithm is studied in a more complex environment using numerical analyses. Different algorithms' lift paths for the same job are illustrated in Fig. 10. For RRT and GA, the shortest distance is searched based on Cartesian coordinates. Specifically, the GA parameters, such as chromosome length, selection probability, crossover probability, mutation probability, population size, and maximum iteration number, are set as 5, 0.5, 0.8, 0.2, 50, and 1000, respectively. The ordinary A* algorithm searches the shortest Manhattan distance in C-space while the improved version uses a heuristic function as (29) and searches in C-space. Unfortunately, RRT and GA cannot determine the shortest path. In addition, their searched paths are difficult to operate with a crane. In contrast, the two A* algorithms' paths use only basic crane movements, thereby promoting ease of operation. This is because these two A* algorithms are executed in C-space, which can naturally account for the boom crane's motion characteristics. Compared with
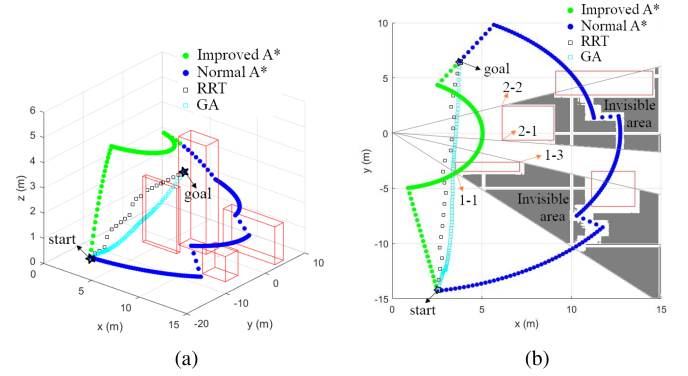
TABLE II
COMPARISON OF THE CRITERIA VALUES OBTAINED BY DIFFERENT A*

Parameters	Improved A*	Ordinary A*	Ratio of improved A* to ordinary A*
Number of expanded node	2252	4734	47.57%
Hosting length (m)	1	1	100.00%
Luffing angle (degree)	25	15	166.67%
Slewing angle (degree)	140	140	100.00%
Consumed energy (J)	771163	1090983	70.69%
Consumed time (s)	362	392.78	92.16%

the path generated by the ordinary A* algorithm, the improved version contains fewer motion switches. Thus, the improved version can eliminate unnecessary motion switches. In addition, the path generated by the improved version will always be visible. In contrast, part of the path generated by the ordinary A* algorithm is located in an invisible area, potentially slowing the operation. Theorem 1 enables the calculation of the invisible part of the path and determining the extra time needed to navigate these areas. The coordinates $(\theta_o, \sigma_o)_{1-1} = (80.2°, -44.4°)$ are for vertex 1 of obstacle 1 (1-1 in Fig. 10). The coordinates of the other vertexes are $(\theta_o, \sigma_o)_{1-3} = (74.8°, -20.3°)$, $(\theta_o, \sigma_o)_{2-1} = (77.7°, -5.9°)$, and $(\theta_o, \sigma_o)_{2-2} = (76.8°, 21.9°)$. The paths generated by the ordinary A* algorithm with coordinate $-44.4° < \sigma < -20.3°$ and $-5.9° < \sigma < 21.9°$ are invisible according to Theorem 1 as their θ values exceed the obstacles. Therefore, $\theta_{iv} = 7°$, $\sigma_{iv} = 51.9°$, and $r_{iv} = 0°$. The extra time spent per luffing and slewing angles are $\Upsilon_\theta = 0.2$ s/°, and $\Upsilon_\sigma = 0.2$ s/°, respectively. The extra time spent in invisible area T_3 is 11.78 s according to (17).

The criteria for evaluating the lift planning performance include the number of expanded nodes, the length of three motions, and the energy and time consumed during the lifting process. Their values, according to different algorithms, are shown in Table II. The efficiency of the graph search algorithm mainly depends on the number of expanded nodes. For the improved A* algorithm, the number of expanded nodes is 47.57% of that generated by the ordinary A* algorithm, indicating that the improved version demonstrates superior computational efficiency. Due to dimension reduction, fewer nodes are expanded when searching with the improved A* algorithm. In addition, the ordinary A* algorithm has a path symmetry problem and,
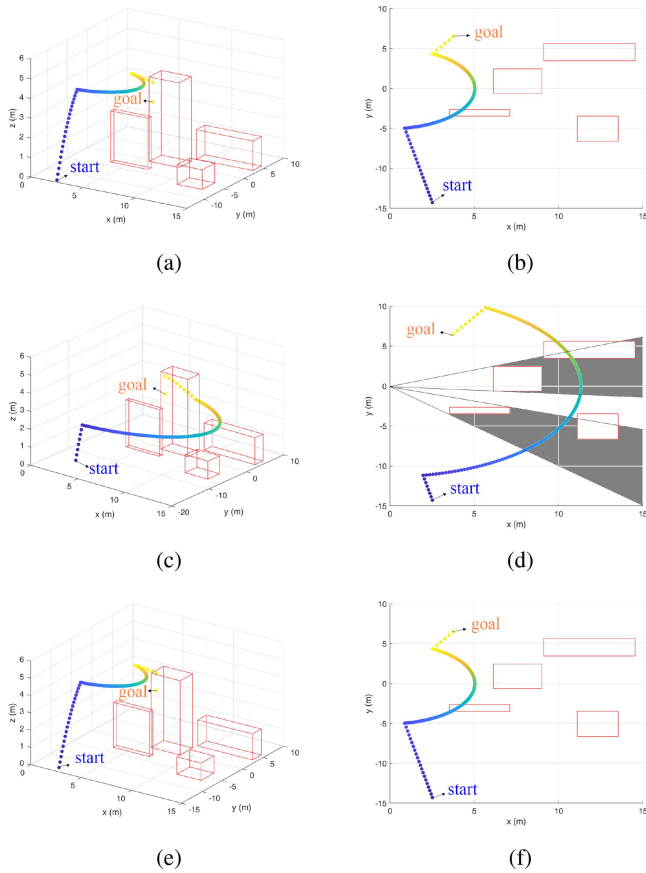
Fig. 11. Paths of the improved A* with three different weights: (a) and (b) $\alpha_e = 1, \alpha_t = 0$; (c) and (d) $\alpha_e = 0, \alpha_t = 1$; (e) and (f) $\alpha_e = 0.5, \alpha_t = 0.5$. (a) Side view. (b) Top view. (c) Side view. (d) Top view. (e) Side view. (f) Top view.

TABLE III
COMPARISON OF THE CRITERIA VALUES WITH DIFFERENT WEIGHTS

Parameters	Scenarios 1 or 3	Scenario 2	Ratio of Scenario 1 to Scenario 2
Hosting length (m)	1	1	100.00%
Luffing angle (degree)	25	15	166.67%
Slewing angle (degree)	140	140	100.00%
Consumed energy (J)	771163	1016185	75.89%
Consumed time (s)	362	352.38	102.73%
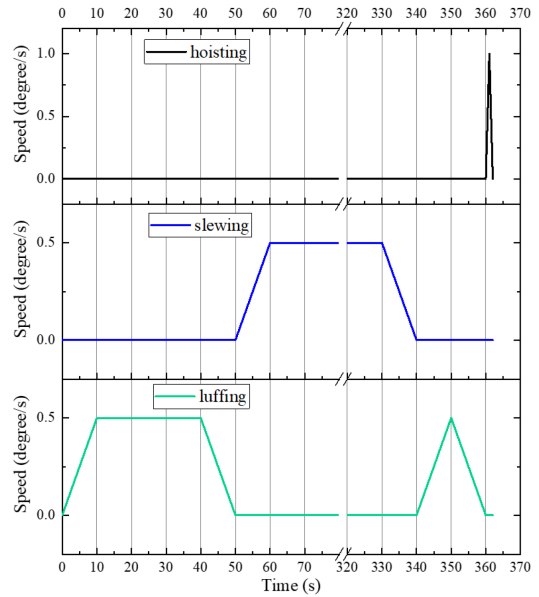
Fig. 12. Speeds of motions in time history for Scenario 1.

consequently, expends considerable effort in the selection with the same heuristic estimation. In contrast, the improved version selects the path with the best energy and time efficiency. As seen in Table II, the improved A* algorithm requires less energy and time than the ordinary version. These observations prove that lift planning in C-Space saves energy and time. The hosting length and slewing angle generated by the improved A* algorithm are the same; meanwhile, the path generated by the ordinary A* algorithm includes an unnecessary motion switch; the improved A* is smoother, saving unnecessary energy and time while motion switching. The invisible part of the path is another factor that caused the lift path generated by the ordinary A* algorithm to take longer to complete.

Fig. 11 compares the paths generated using the improved A* algorithm across three different scenarios: Scenario 1, only energy criterion ($\alpha_e = 1, \alpha_t = 0$); Scenario 2, only time criterion ($\alpha_e = 0, \alpha_t = 1$); and Scenario 3, a combination of normalized energy and time ($\alpha_e = 0.5, \alpha_t = 0.5$), respectively. Scenarios 1 and 3 produced the same path; however, Scenario 2 was different. Table III includes comparisons of the different scenarios. Scenarios 1 and 3 consumed less energy than Scenario 2. From Fig. 11, compared with Scenario 2, the crane slews under larger θ in Scenarios 1 and 3. According to (10), Scenarios 1 and 3 consume less energy during slewing. Scenarios 1 and 3 consume

more time than Scenario 2 (see Table III), likely because of their greater luffing angles. Due to payload sway limitations, we assume the crane moves steadily at a fixed speed. We assume that the rate of speed changes during motion switching is a fixed value according to the crane's engine power. Consequently, more luffing angles necessitate more luffing time. When the crane's configuration sequence is identified, its motion information can be implied. Motion speeds from Scenario 1 are illustrated in Fig. 12.

VI. CONCLUSION

We proposed a dynamic 3-D lift planning method that can automatically determine a lift path while considering multiple factors. Real-world lift plans have been broken down and presented as mathematical models that include comprehensive objectives and detailed constraints. The proposed energy and time consumption models quantify potential moving costs while lifting for further analysis and evaluation. Two essential boom crane characteristics were proposed to distinguish lift planning from other path planning, and an enveloping method of obstacles was derived accordingly. We proposed a dimension reduction method to reduce the improved A* algorithm's necessary calculation time, then proved its admissibility and optimality. The experimental results demonstrated that the proposed lift planning method comprehensively considered multiple objectives and generated a qualified path for actual lifting. The generated path

considered both energy and time while satisfying the requirements of safety, visibility, and ease of operation. Our complex environmental simulations demonstrated that the improved A* algorithm is capable of generating a superior path compared to the ordinary A* algorithm. This optimized path required less energy and time. Future lift planning processes will need to consider dynamic obstacles using motion prediction methods.

REFERENCES

[1] G. O. Tysse, A. Cibicik, and O. Egeland, "Vision-based control of a knuckle boom crane with online cable length estimation," *IEEE/ASME Trans. Mechatronics*, vol. 26, no. 1, pp. 416–426, Feb. 2021.

[2] M. Li, H. Chen, and R. Zhang, "An input dead zones considered adaptive fuzzy control approach for double pendulum cranes with variable rope lengths," *IEEE/ASME Trans. Mechatronics*, vol. 27, no. 5, pp. 3385–3396, Oct. 2022.

[3] B. Zhao, H. Ouyang, and M. Iwasaki, "Motion trajectory tracking and sway reduction for double-pendulum overhead cranes using improved adaptive control without velocity feedback," *IEEE/ASME Trans. Mechatronics*, vol. 27, no. 5, pp. 3648–3659, Oct. 2022.

[4] Z. Zhang and W. Pan, "Lift planning and optimization in construction: A thirty-year review," *Automat. Construction*, vol. 118, 2020, Art. no. 103271.

[5] H. Yin, Y.-H. Chen, J. Huang, and H. Lü, "Tackling mismatched uncertainty in robust constraint-following control of underactuated systems," *Inf. Sci.*, vol. 520, pp. 337–352, 2020.

[6] S. Hu, Y. Fang, and Y. Bai, "Automation and optimization in crane lift planning: A critical review," *Adv. Eng. Informat.*, vol. 49, 2021, Art. no. 101346.

[7] S. Kang and E. Miranda, "Planning and visualization for automated robotic crane erection processes in construction," *Automat. Construction*, vol. 15, no. 4, pp. 398–414, 2006.

[8] S. H. Han, S. Hasan, A. Bouferguène, M. Al-Hussein, and J. Kosa, "Utilization of 3D visualization of mobile crane operations for modular construction on-site assembly," *J. Manage. Eng.*, vol. 31, no. 5, 2015, Art. no. 04014080.

[9] S.-C. Kang, H.-L. Chi, and E. Miranda, "Three-dimensional simulation and visualization of crane assisted construction erection processes," *J. Comput. Civil Eng.*, vol. 23, no. 6, pp. 363–371, 2009.

[10] S. Pooladvand, H. Taghaddos, A. Eslami, A. N. Tak, and U. Hermann, "Evaluating mobile crane lift operations using an interactive virtual reality system," *J. Construction Eng. Manage.*, vol. 147, no. 11, 2021, Art. no. 04021154.

[11] C. Zhang and A. Hammad, "Multiagent approach for real-time collision avoidance and path replanning for cranes," *J. Comput. Civil Eng.*, vol. 26, no. 6, pp. 782–794, 2012.

[12] X. Wang, Y. S. Lin, D. Wu, C. W. Zhang, and X. K. Wang, "Path planning for crane lifting based on bi-directional RRT," *Adv. Mater. Res.*, 2012, vol. 446, pp. 3820–3823.

[13] Y. Lin, D. Wu, X. Wang, X. Wang, and S. Gao, "Lift path planning for a nonholonomic crawler crane," *Automat. Construction*, vol. 44, pp. 12–24, 2014.

[14] A. R. Soltani, H. Tawfik, J. Y. Goulermas, and T. Fernando, "Path planning in construction sites: Performance evaluation of the Dijkstra, A*, and GA search algorithms," *Adv. Eng. Inform.*, vol. 16, no. 4, pp. 291–303, 2002.

[15] M. A. D. Ali, N. R. Babu, and K. Varghese, "Collision free path planning of cooperative crane manipulators using genetic algorithm," *J. Comput. Civil Eng.*, vol. 19, no. 2, pp. 182–193, 2005.

[16] Y.-C. Chang, W.-H. Hung, and S.-C. Kang, "A fast path planning method for single and dual crane erections," *Automat. Construction*, vol. 22, pp. 468–480, 2012.

[17] S. Hu, Y. Fang, and H. Guo, "A practicality and safety-oriented approach for path planning in crane lifts," *Automat. Construction*, vol. 127, 2021, Art. no. 103695.

[18] J. An, M. Wu, J. She, and T. Terano, "Re-optimization strategy for truck crane lift-path planning," *Automat. Construction*, vol. 90, pp. 146–155, 2018.

[19] M. Hussein and T. Zayed, "Crane operations and planning in modular integrated construction: Mixed review of literature," *Automat. Construction*, vol. 122, 2021, Art. no. 103466.

[20] T. Zhang, J. Wang, and M. Q.-H. Meng, "Generative adversarial network based heuristics for sampling-based path planning," *IEEE/CAA J. Automatica Sinica*, vol. 9, no. 1, pp. 64–74, Jan. 2022.

[21] P. Cai, Y. Cai, I. Chandrasekaran, and J. Zheng, "Parallel genetic algorithm based automatic path planning for crane lifting in complex environments," *Automat. Construction*, vol. 62, pp. 133–147, 2016.

[22] Z. Lei, S. Han, A. Bouferguúne, H. Taghaddos, U. Hermann, and M. Al-Hussein, "Algorithm for mobile crane walking path planning in congested industrial plants," *J. Construction Eng. Manage.*, vol. 141, no. 2, 2015, Art. no. 05014016.

[23] H. R. Reddy and K. Varghese, "Automated path planning for mobile crane lifts," *Comput. Aided Civil Infrastructure Eng.*, vol. 17, no. 6, pp. 439–448, 2002.

[24] N. Kayhani, H. Taghaddos, A. Mousaei, S. Behzadipour, and U. Hermann, "Heavy mobile crane lift path planning in congested modular industrial plants using a robotics approach," *Automat. Construction*, vol. 122, 2021, Art. no. 103508.

[25] L. Jiang, S. Liu, Y. Cui, and H. Jiang, "Path planning for robotic manipulator in complex multi-obstacle environment based on improved_RRT," *IEEE/ASME Trans. Mechatronics*, vol. 27, no. 6, pp. 4774–4785, Dec. 2022.

[26] K. Shu et al., "Autonomous driving at intersections: A behavior-oriented critical-turning-point approach for decision making," *IEEE/ASME Trans. Mechatronics*, vol. 27, no. 1, pp. 234–244, Jan. 2022.

[27] T. Liu, W. Xu, T. Yang, and Y. Li, "A hybrid active and passive cable-driven segmented redundant manipulator: Design, kinematics, and planning," *IEEE/ASME Trans. Mechatronics*, vol. 26, no. 2, pp. 930–942, Apr. 2021.

[28] P. Á. Sivakumar, K. Varghese, and N. R. Babu, "Automated path planning of cooperative crane lifts using heuristic search," *J. Comput. Civil Eng.*, vol. 17, no. 3, pp. 197–207, 2003.

[29] M. Likhachev, G. J. Gordon, and S. Thrun, "ARA*: Anytime A* with provable bounds on sub-optimality," *Adv. Neural Inf. Process. Syst.*, vol. 16, 2003.
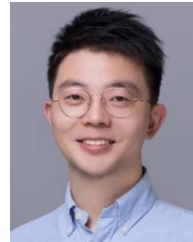
Zheshuo Zhang (Member, IEEE) received the Ph.D. degree in civil engineering from Science and Engineering Faculty, Queensland University of Technology, Brisbane, QLD, Australia, in 2019.

He is currently an Associate Researcher with Zhejiang University City College, Hangzhou, China. He was a Research Fellow with the College of Mechanical and Vehicle Engineering, Hunan University, Changsha, China. His research interests include planning, optimization, adaptive robust control, and precise control of uncertain nonlinear systems.

Bangji Zhang received the M.E. and Ph.D. degrees in mechanical engineering from Hunan University, Changsha, China, in 1999 and 2010, respectively.

He is currently a Professor with Zhejiang University City College, Hangzhou, China. He was a Professor with the College of Mechanical and Vehicle Engineering, Hunan University, a Research Fellow with the State Key Laboratory of Advanced Design and Manufacturing for Vehicle Body, and a Visiting Scholar with the University of Technology Sydney, Ultimo, NSW, Australia.

Wen Hu received the M.S. and Ph.D. degrees in mechanical engineering from Hunan University, Changsha, China, in 2018 and 2022, respectively.

He is currently a Postdoctoral Research Fellow with Tsinghua University, Beijing, China. He was a visiting Ph.D. student with the Department of Mechanical and Mechatronics Engineering, University of Waterloo. His research interests include driving risk assessment, decision making, and trajectory planning in intelligent vehicle.

Rui Zhou received the M.Sc. degree in automobile engineering from the Technical University of Braunschweig, Braunschweig, Germany, in 2014. He is currently working toward the Ph.D. degree in intelligence science and systems with the Macau University of Science and Technology, Macau.

He is currently an R&D Director with Waytous, Inc., Qingdao, China. His research interests include autonomous vehicle, test area for connected vehicle, and functional safety.

Hui Yin (Member, IEEE) received the B.S. and Ph.D. degrees in mechanical engineering from Hunan University, Changsha, China, in 2012 and 2018, respectively.

He was a visiting scholar with the Georgia Institute of Technology, Atlanta, GA, USA. He is currently an Associate Professor with Hunan University. His research interests include mechanical system dynamics, adaptive robust control, fuzzy engineering, structural optimization, and uncertainty management.

Dongpu Cao (Member, IEEE) received the Ph.D. degree in mechanical and industrial engineering from Concordia University, Montreal, QC, Canada, in 2008.

He is currently a Professor with Tsinghua University, Beijing, China. His research interests include driver cognition, automated driving, and cognitive autonomous driving. He has authored or coauthored more than 200 papers and three books.

Dr. Cao was the recipient of the SAE Arch T. Colwell Merit Award in 2012, IEEE VTS 2020 Best Vehicular Electronics Paper Award, and six best paper awards from international conferences. He has was the Deputy Editor-in-Chief for IET Intelligent Transport Systems Journal, and an Associate Editor for IEEE TRANSACTIONS ON VEHICULAR TECHNOLOGY, IEEE TRANSACTIONS ON INTELLIGENT TRANSPORTATION SYSTEMS, IEEE/ASME TRANSACTIONS ON MECHATRONICS, IEEE TRANSACTIONS ON INDUSTRIAL ELECTRONICS, IEEE/CAA JOURNAL OF AUTOMATICA SINICA, IEEE TRANSACTIONS ON COMPUTATIONAL SOCIAL SYSTEMS, and *ASME Journal of Dynamic Systems, Measurement and Control*. He is an IEEE VTS Distinguished Lecturer.